JOURNAL OF CATALYSIS 147, 140–155 (1994)

Catalysis over Porous Anodic Alumina Catalysts

G. Patermarakis and C. Pavlidou

Laboratory of Physical Chemistry and Applied Electrochemistry, Department of Chemical Engineering, National Technical University of Athens, Greece

Received August 6, 1991; revised August 11, 1993

Porous alumina films with a high pore surface density, of the order of $10^{10}/cm^2$, were prepared on Al metal by the galvanostatic anodic oxidation of Al metal in a thermostated, nonstirred bath of H_2SO_4 solution, 15% w/v, at various bath temperatures and current densities that resulted in different oxide film thicknesses, in order to be used as catalysts. Structural features such as pore base diameter, porosity, and total and specific real surface were determined by means of kinetic data obtained from the Al_2O_3 film growth. The catalytic behaviour of the porous anodic Al_2O_3 films was investigated by using the decomposition of HCOOH as a test reaction in the temperature range 270–390°C. The catalytic decomposition of HCOOH was found to be a dehydration reaction of zero order with respect to the partial pressure of HCOOH at an operation pressure of 1 atm. After some initial catalyst deactivation, the kinetic parameters of the catalytic dehydration, namely activation energy, frequency factor, total activity (referred to a constant geometric film surface area), and specific activity (expressed either per g of oxide mass or per m^2 of real surface) at 350°C were found to be strongly affected by film thickness and bath temperature. Anodic Al_2O_3 films modified by hydrothermal treatment gave consistently higher values of the kinetic parameters, while the span of their variation with film thickness was significantly reduced in comparison to the untreated films. Also, the initial deactivation was prevented to a significant extent. This catalytic behaviour was satisfactorily explained on the basis of the microcrystalline nature of the oxide, the presence of electrolyte anions incorporated inside the oxide bulk during film growth, and the heterogeneity of the oxide surface present along the walls of conical pores.

INTRODUCTION

Aluminium oxides in the form of either porous or nonporous films on Al metal substrate can be produced electrolytically by the electrochemical (anodic) oxidation of Al metal and are usually called anodic aluminas. These Al_2O_3 films have a cellular structure and the choice of electrolyte determines the nature of the product film. Nonporous (barrier type) Al_2O_3 films are formed in electrolytes which do not dissolve the Al_2O_3 produced (boric acid solution, ammonium borate or tartrate aqueous solutions, ammonium tetraborate in ethylene glycol, citric acid, malic acid), while porous Al_2O_3 films are formed in electrolytes which dissolve the produced Al_2O_3 sparingly (sulphuric, phosphoric, oxalic acids) (1, 2). The thickness of the nonporous films is approximately proportional to the imposed voltage (≃14 Å/V) and can reach up to 1 μm, while the thickness of porous films can reach many tens of μm.

The structure of porous Al_2O_3 films has been characterized by a close-packed array of approximately hexagonal, columnar cells each of which contains an elongated, roughly cylindrical pore extending between the film's external surface and the Al_2O_3/Al interface, where it is sealed by a thin, compact, barrier type oxide layer. This structure is schematically depicted in Fig. 1. The structural features such as pore diameter and cell or pore surface concentration depend on the choice of electrolyte and the conditions of anodic oxidation. Pore diameter generally varies from a few Å up to a few hundred Å, while the pore surface concentration is very high, of the order of $10^{10}/cm^2$ of anodized metal geometric surface. The application of either porous or nonporous anodic Al_2O_3 films in catalysis research has recently become the object of investigation and the results seem promising (3).

Nonporous (4–7) and porous (8, 9) anodic aluminas were studied as model catalysts. Platinum (4, 5, 7) and palladium (6) suspended over nonporous films were examined in order to investigate their behaviour in thermal and reactive treatment. It has been reported that by different methods (8, 9) parallel cylindrical pores in thin films with a pore diameter ranging between 15 and 200 Å in size can be obtained. Porous anodic aluminas produced by anodizing Al wires (subsequently cut for the purpose of producing cylindrical catalyst particles having metallic cores) were employed in the dehydrogenation of 2-propanol and the isomerisation of *n*-butene. They exhibited a 30-fold higher specific activity than that of bulk γ-Al_2O_3 in the dehydration of 2-propanol and also a higher activity in the isomerisation reaction (10, 11).

Platinum sintering on nonporous anodic Al_2O_3 and the effect on Pt/Al_2O_3 catalysts of chemical and thermal treatment in various media have been studied (12–14), while the hydrogenolysis of methylcyclopentane was also tested

0021-9517/94 $6.00

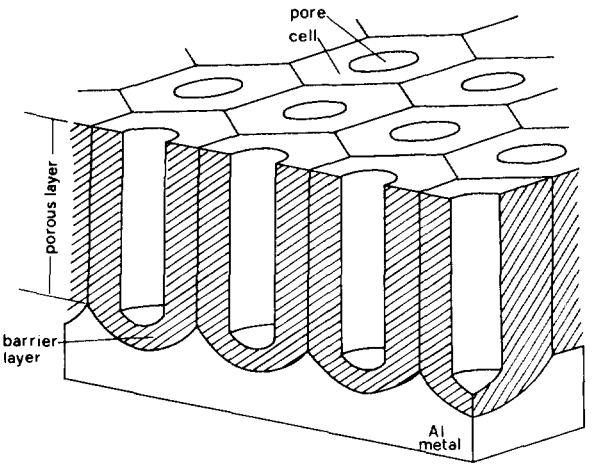

FIG. 1. Schematic representation of the hexagonal columnar cell structure of porous anodic Al_2O_3 films.

on these catalysts when platinum particles of varying sizes were attached (14), as well as on island stage ultrathin platinum films of defined orientation on anodic amorphous Al_2O_3 (15). Porous anodic Al_2O_3 films have been tested in the HCOOH decomposition reaction (16, 17) and a significantly higher dehydrating efficiency as compared to that exhibited by chemically prepared Al_2O_3 has been reported (16). In the present study porous anodic Al_2O_3 films were prepared under various anodization conditions, producing different oxide thicknesses in H_2SO_4 electrolyte, which, among other electrolytes yields Al_2O_3 films with the highest surface pore concentration (18), and their structure was determined. HCOOH decomposition was investigated as a test reaction in view of its previous widespread use as a model reaction for catalytic selectivity (19). An interpretation of the catalytic behaviour of anodic aluminas was also attempted.

EXPERIMENTAL

1. Preparation and Characterization of Anodic Aluminas

An Al metal sheet of 0.5 mm in thickness was used for the preparation of anodic alumina catalysts. Its composition was Al 99.5%, Fe 0.26%, Si 0.2%, and the remainder consisted of traces of other elements.

Specimens, 30 × 50 mm, were cut out from the sheet. Each specimen was divided into 25 × 5 mm strips parallel to the 30 mm specimen side kept together by a 50 × 5 mm strip parallel to the 50 mm upper specimen side. Each specimen had a tailing end 50 × 10 mm perpendicular to this strip, and stemming from the middle of the 50 mm side. Prior to anodic oxidation (anodization), specimens were rinsed with water and ethanol, degreased with xylol, and dried, while their tailing ends, 50 mm in length, were covered with an insulating varnish, leaving bare only a small part at the edge for the electrical connection. The anodic oxidation of each Al specimen was carried out galvanostatically in a thermostated, nonstirred bath of aqueous H_2SO_4 15% w/v solution. Two Pb sheets having the same dimensions as the Al specimen were used as cathodes placed symmetrically on either side and parallel to the Al electrode at a distance of 50 mm.

After the anodic oxidation had been completed, the oxidized Al specimens were rinsed with water and neutralized with 0.1 *M* NaOH to remove H_2SO_4 accumulated in the pores and the maximum possible amount of SO_4^{2-} anions adsorbed on the pore wall surface. Specimens were rinsed again with water, dried in an air stream, and stored in a desiccator prior to use. To obtain representative mean values of the main structural features of the films, the mass and thickness were determined by methods previously described (20).

The H_2SO_4 bath solution obtained after anodic oxidation was analyzed by atomic absorption spectrometry to determine the amount of Fe dissolved during electrolysis and hence to derive the amount of Fe_2O_3 present in the Al_2O_3 oxide layer. Despite the fact that the percentage of Fe in the Al metal was very low, the presence of Fe_2O_3 might influence the results of the catalytic test reaction, since Fe_2O_3 is both a strong dehydrogenating and a dehydrating catalyst (21). The SiO_2 content, on the other hand, could not influence the catalytic results, since its activity is dehydrating in character and low in comparison to that of alumina (22).

2. Experimental Setup and Procedure for the Catalytic Test Reaction over Anodic Aluminas

The strips into which the Al metal was divided prior to anodization were separated by cutting appropriately the strip keeping them together at the top of the Al specimen. The ten 30 × 5 mm strips thus formed, with a total oxidized geometric surface area of 33 cm^2, composed the catalyst supplied to the reactor. For the HCOOH decomposition a classical Schwab differential microreactor (23) was employed. The setup comprised the container of liquid HCOOH, the evaporator, the reactor chamber, and the condenser where the unreacted gaseous HCOOH and the product H_2O were condensed.

The reactor operated differentially as a continuous flow system. The operation conditions were such that the dilution of the condensed HCOOH by the product H_2O was always negligible, permitting the mixing of the condensates with the HCOOH in the container and the continuous recirculation of HCOOH during each run, while the rate of HCOOH decomposition was not affected. The reaction rate was measured by the flow rate of the produced gases at room temperature. The setup operated at atmospheric pressure.

Measurements of reaction rate were taken at various reaction temperatures by a dynamic method. The reactor temperature was raised linearly with time, initially at a rate of ≈10°C/min from room temperature up to a temperature at which the HCOOH decomposition produced a measurable reaction rate, this temperature being always >270°C. Then it was regulated to increase at a rate of ≈2.5°C/min up to a desired temperature, different for the various catalysts employed but always ≤390°C, which was considered to be the drying temperature of the anodic alumina, and then to decrease at the same rate to >270°C, as above, in order to reveal any hysteresis phenomena in the reaction rate measurements.

These phenomena could arise from the finite rate of heat transfer inside the reactor chamber, which at high rates of change of reaction temperature could produce appreciable differences between the true average reaction temperature and that measured. Since the HCOOH decomposition rate at a given temperature initially showed a significant decrease with operation time, indicating catalyst deactivation, the above temperature scanning procedure was repeated twice more. The difference in reaction rates between the first and second scanning procedures was obvious but between the second and third ones no appreciable difference in reaction rate appeared.

This serves to show that the total initial catalyst deactivation was approximately complete by the end of the second temperature scanning operation, i.e., within 120–200 min from the beginning of each experiment, beyond which changes in the reaction rate were negligible. Further temperature scanning yielded rate measurements essentially coinciding with those of the third scanning operation while hysteresis phenomena between scannings were not perceptible. Hence, reaction rate measurements at various temperatures obtained during the thrid scanning operation over the reaction temperature range were considered to be reliable and were taken into consideration throughout the present work.

Once HCOOH catalytic decomposition experiments had been completed, catalysts were dried and neutralized with 0.1 *M* NaOH. Subsequently they were modified by hydrothermal treatment in boiling H_2O for a fairly long time, 4.5 hr, thus ensuring complete or nearly complete hydration (24), and were allowed to dry in the atmosphere for ≈10 min to allow for the evaporation of free H_2O molecules on the oxide surface. These modified Al_2O_3 film catalysts, without any further treatment, were again tested in the HCOOH decomposition reaction as described above.

RESULTS AND DISCUSSION

1. Structure of the Porous Anodic Alumina Films

The variation of the film thickness (h) and oxide mass (m) spread over the 33 cm² oxidized geometric surface area of anodized Al specimens (S_g) with the anodization time interval (t) at bath temperatures (T_b) = 25, 30, and 40°C and current densities (i) = 5, 15, and 35 mA/cm² is shown in Figs. 2a and 2b. The film thickness increases

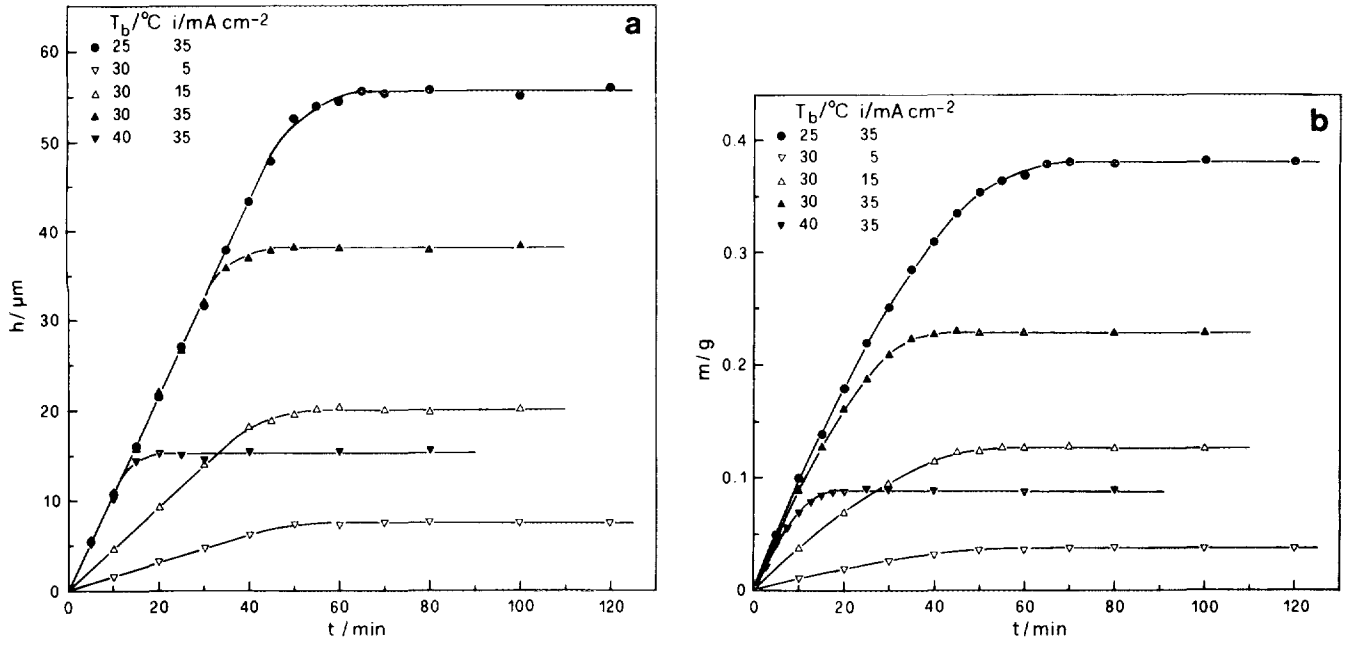

FIG. 2. Variation of film thickness (a) and oxide mass spread over the 33 cm² geometric surface area of the anodized Al metal specimens (b) with anodization time at various bath temperatures and current densities.

linearly up to a particular anodization time (t_1) or film thickness h_1 for each pair of T_b and i; then the rate of thickness increase slows down until another anodization time (t_c), also particular for each pair of T_b and i, where it becomes zero. Beyond t_c the thickness remains constant, h_c. The mass of oxide film also increases with anodization time but with a continuously decreasing rate up to t_c, where the rate also becomes zero. Beyond t_c a constant mass m_c is observed.

The surface concentration of pores (n) is independent of T_b; it is strictly defined by current density, being for example 3.69×10^{10}, 2.93×10^{10}, and 2.30×10^{10} pores/cm^2 for i = 5, 15, and 35 mA/cm^2, respectively (20). The mass of the oxide film was found (20) to be satisfactorily described by the kinetic equation

$$m = kit - \lambda_1 t \exp(\lambda_2 t) \quad \text{for } t \leq t_c, \qquad [1]$$

where k is a constant independent of i and T_b, while λ_1 and λ_2 are parameters depending on T_b and i, which are related to the pore base mean diameter (D_0) and the rate of pore wall oxide dissolution, defined as the thickness of pore wall material dissolved per unit of time (k_d), by the equations

$$\lambda_1 = 4^{-1} ki\pi n D_0^2 \qquad [2]$$

$$\lambda_2 = 2k_d D_0^{-1}. \qquad [3]$$

The true shape of pores anticipated by Eqs. [1], [2], and [3] is to a good approximation that of truncated cone. A schematic representation (not to scale) of the section of an oxide cell with the maximum limiting film thickness is given in Fig. 3a, where the barrier layer (ACDEGKA), the pore wall material (ABCA and GEFG), the cell boundaries (BC and FE), the conical pore shape (FGAB), and the cross-section of the pore wall surface (AB or GF) are depicted. Using Eq. [1] the porosities p and p' (where p = void volume per gram of oxide mass and p' = void volume per unit of total film volume) are given by the equations

$$p = S_g h(kit - \lambda_1 t \exp(\lambda_2 t))^{-1} - d_c^{-1} \text{ for } t \leq t_c,$$
$$\text{and } p = p(t_c) \text{ for } t > t_c, \qquad [4]$$

$$p' = 1 - (S_g h d_c)^{-1} (kit - \lambda_1 \exp(\lambda_2 t)) \text{ for } t \leq t_c$$
$$\text{and } p' = p'(t_c) \text{ for } t > t_c, \qquad [5]$$

where d_c is the density of compact anodic Al_2O_3, which was found to be 3.42 g/cm^3 (20). The total real oxide surface, S, of conical pores present on the anodized geometric surface area of Al metal, S_g, is given by the

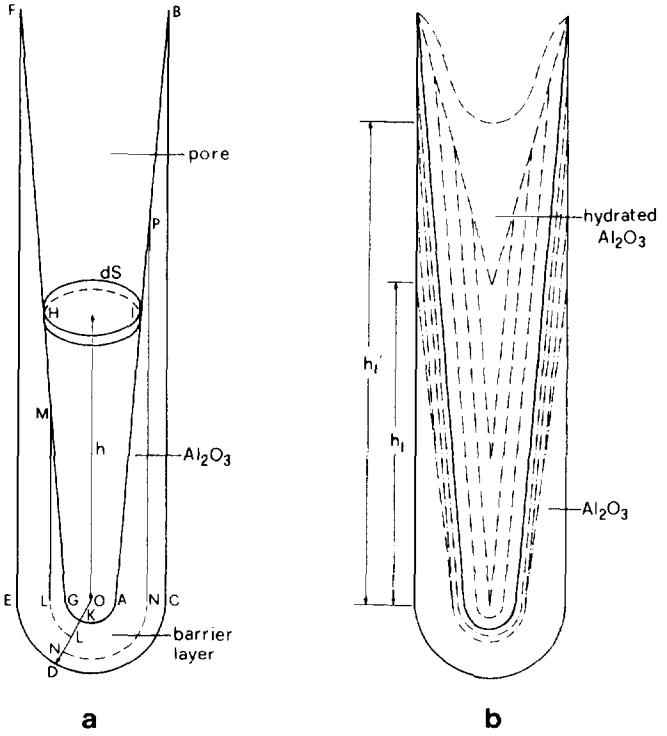

FIG. 3. Schematic representation of a section parallel to the pore axis of an elongated, columnar cell of a film with the maximum limiting thickness (a) and of the hydration process of pore wall oxide (b) where (—), (---) and (-·-) depict respectively the initial surface of pore walls and cell boundaries, the surfaces of the hydrated layer on pore walls, and the interfaces of the Al_2O_3/hydrated oxide layer during oxide hydration.

equation

$$S = 4\lambda_1 t(d_c D_0)^{-1}(1 + 2^{-1}\lambda_2 t), \qquad [6]$$

which is accurate for $t \leq t_1$, while for $t > t_1$ a better estimate is given by the formula

$$S = 2^{-1}(n\pi S_g h)^{1/2}[(\lambda_1 S_g h)^{1/2}(ki)^{-1/2} + (3S_g h(4 - \lambda_1(ki)^{-1}) - 12md_c^{-1})^{1/2}]. \qquad [7]$$

By fitting experimental m values in Eq. [1], λ_1 and λ_2 were calculated as $\lambda_1 = 6.4 \times 10^{-4}$, 13.5×10^{-4}, 27.3×10^{-4}, 24.0×10^{-4}, and 33.7×10^{-4} g/min and $\lambda_2 = 9.9 \times 10^{-3}$, 14.2×10^{-3}, 21.7×10^{-3}, 15.4×10^{-3}, and 44.5×10^{-3} min^{-1}, for i = 5, 15, 35 mA/cm^2 at 30°C and i = 35 mA/cm^2 at 25 and 40°C, respectively, by means of which D_0 was found to be 356, 335, 352, 330, and 391 Å accordingly; D_0 therefore increases considerably with T_b and varies insignificantly with i. These results show that the thickness of the barrier layer decreases with increasing T_b and decreasing i.

The pore diameter at the pore mouths of films with thickness $\approx h_1$ becomes comparable to cell size. Since

pores become gradually interconnected at the film surface a reasonable approximation of pore diameter at pore mouths is the mean value of the lower and higher cell diameter values in Fig. 1, which calculated from n values is found to be 603, 676, and 763 Å at 5, 15, and 35 mA/cm^2, respectively. For films with thicknesses $h_1 < h < h_c$ an external thin layer with thickness $h - h_1$ exists. Due to the structure of the oxide and the mechanism of its growth (20), the variable diameter of pores along their length corresponding to this layer must be nonuniform over the whole film surface.

A fraction of the pores will have a diameter ranging from the above values up to values defined by the higher hexagon cell diameters. Another fraction of the pores will have diameters corresponding to pore-sizes produced from a small number of interconnected initial pores in the thin external layer with thickness $h - h_1$ and values of the order of 10^3 Å. Finally, the local interconnection of many initial pores may produce pores inside this thin layer which will have higher diameter values, of the order of 10^4 or 10^5 Å. Nevertheless, for most of the pore length, h_1, the pore diameter at every point along the pore length will be uniform for all pores; this is a basic feature of the structure of the porous anodic Al_2O_3 films (1, 2). The contribution of the thin external layer, of thickness $h - h_1$, to porosity and real surface is certainly insignificant when compared with the contribution of the film layer of thickness h_1.

It is noted that different values of pore base and pore mouth diameters, different shapes, and hence different models for oxide porosity can be obtained by employing other electrolytes and conditions of anodization (1, 2, 8, 9, 25).

The variation of the values of certain structural parameters, i.e., porosity (p'), total real surface, and specific real surface ($s = Sm^{-1}$) of the Al_2O_3 film with t at various T_b's and i's, calculated from Eqs. [1], [5], [6], and [7] are shown in Figs. 4a, 4b, and 4c, respectively. All p', S, and s parameters vary similarly with t. An inflection point appears at $\simeq t_1$. Beyond t_c the values of p', S, and s remain approximately constant. For the same film thickness the increase in T_b and the decrease in i exert a positive effect on p', S, and s. For $t > t_c$ the values of S generally increase with decreasing T_b and increasing i owing primarily to the increase in the maximum limiting film thickness h_c; s, however, generally increases in the opposite direction, i.e., with increasing T_b and decreasing i. In the case of p' at $t > t_c$ its dependence on T_b and i is somewhat different. Although some slight change of p' is observed with T_b and i its variation is not significant, p' being always between 0.4 and 0.55. A similar variation of p with t, T_b, and i was also verified.

In contrast to the above method, real surface determination by the BET method of all the prepared anodic Al_2O_3 films was tedious, mainly due to their large number. For comparison, however, the real surface of oxides prepared at $T_b = 30$°C and $i = 15$ and 35 mA/cm^2 with thickness h_c was measured by the BET method and essentially coincided with that determined by the method applied, proving its validity.

2. *The Nature of the Oxide and the Heterogeneity of the Pore Wall Surface*

It was shown earlier (20) that the porous anodic Al_2O_3 films prepared in H_2SO_4 electrolyte are essentially dry materials. The percentage of water as molecular water or as OH groups incorporated inside the compact pore wall oxide is lower than 1% and is relatively easily removed on heating (24). Its concentration inside the barrier layer must decrease from the pore base surface towards the Al/Al_2O_3 interface.

The compact oxide around the pore walls was proved by XRD and IR techniques to be a microcrystalline material consisting of crystallites with an average size much lower than 100 Å (24). Their size was found elsewhere to be consistently $\simeq$40 Å as determined by an NMR spectroscopic study (26). The average size of crystallites is expected to vary with anodic oxidation conditions such as T_b and i, increasing with the former and decreasing with the latter. Crystallite size should also vary along the cross section of the barrier layer (25) increasing along the direction from pore base surface to the Al_2O_3/Al interface (i.e., along KD in Fig. 3a).

It is reasonable to suppose that at such extremely low crystallite sizes, a few tens of Å, an optimum crystallite size ought to exist from the point of view of catalytic activity. Below this optimum size the crystallite surface probably becomes incapable of creating and retaining with adequate strength the appropriate adsorbed species for subsequent reaction; i.e., despite the enlarged number of disordered surface atoms/active centres per unit of crystallite volume, their intensity diminishes. Consequently, the number of actual catalytically active centres also diminishes. Above the optimum size both the number and the intensity of active centres diminish due to the reduction in the number of disordered surface atoms. The experimental results agree with the assumption that crystallite sizes are always larger than the optimum.

Electrolyte anions are always incorporated inside the barrier layer during its formation. The bulk concentration of electrolyte anions incorporated into the film varies at large not only with the kind of electrolyte but with respect to the same electrolyte as well (1, 2, 18). The incorporation of SO_4^{2-} is generally the largest among other electrolyte anions. Its amount was found to be even up to $\simeq$11 wt% of the oxide mass. The variation of electrolyte anion concentration inside the initially formed barrier layer at the

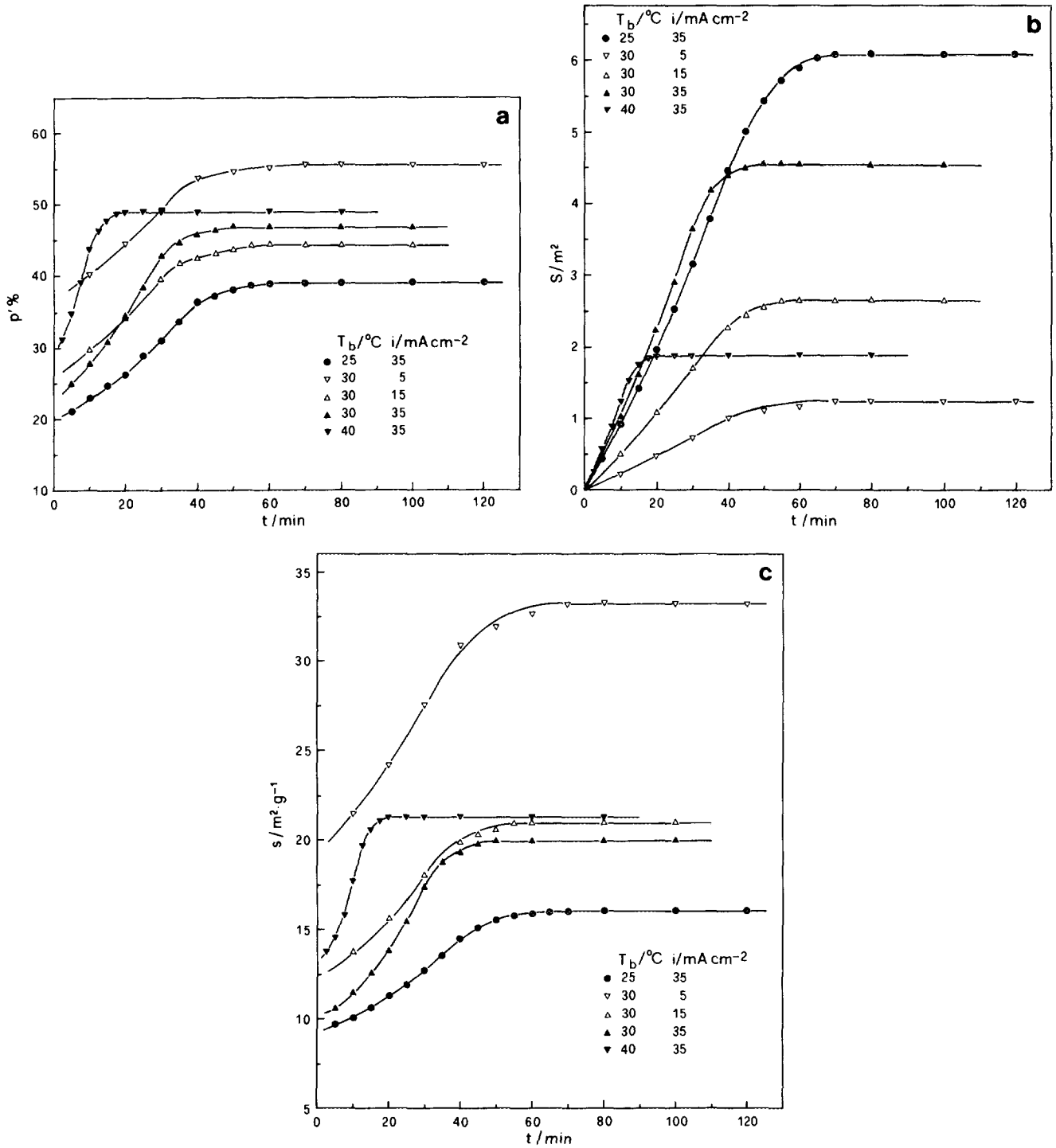

FIG. 4. Dependence of (a) the percentage v/v porosity, (b) the total real surface of oxide present on the 33 cm^2 geometric surface area of Al metal anodically oxidized, and (c) the specific real surface area on anodization time (t) at various bath temperatures and current densities.

very early stages of anodization and prior to the appearance of the porous layer was examined by an Auger electron spectroscopy study (27) for films prepared in H_2SO_4 electrolyte. The SO_4^{2-} concentration appeared to be at a maximum near the oxide surface and gradually decayed with decreasing rate on approaching the Al_2O_3/Al interface.

The concentration of electrolyte anions, also SO_4^{2-} in

the present case, is expected to vary in a similar fashion across the barrier layer. The SO_4^{2-} concentration probably becomes zero at a point, N, prior to the Al_2O_3/Al interface. It appears that, generally, the increase in SO_4^{2-} concentration keeps pace with the decrease in crystallite size, so that SO_4^{2-} anions are situated on intercrystallite surfaces rather than embedded inside crystallites. The concentration of SO_4^{2-} inside the barrier layer must also increase with i and T_b considerably in the vicinity of pore base surface (which is probably relatively free of SO_4^{2-} due to the removal of SO_4^{2-} by the neutralizing solution) and at any point at a constant distance away from the pore base surface present inside the barrier layer.

The mechanism of porous film formation provides that the nature of the oxide at each point on the pore wall surface (i.e., M) will be identical to that of the corresponding point in the barrier layer oxide (i.e. L), Fig. 3a, as the latter point becomes a surface point on dissolution of pore wall oxide by the electrolyte during the formation of the porous oxide layer. The above change in crystallite sizes and in the SO_4^{2-} concentration and hence in the oxide nature across the barrier layer are also extrapolated for a thin oxide layer of thickness comparable to crystallite sizes lying in the vicinity of the pore wall surface, creating a corresponding surface heterogeneity.

Previously, in the case of barrier type films, it was shown that in the oxide mass there existed an oxygen surplus (28), presumably in an adsorbed state within film cavities, but it could also be attributed to a stoichiometric oxygen excess. Such stoichiometry defects may also occur inside the barrier layer of the porous films. The oxygen atom surplus is similarly expected, as is the incorporated SO_4^{2-}, to decrease across the barrier layer and probably becomes zero at a point prior to the Al_2O_3/Al interface, beyond which a surplus of aluminium atoms may be established.

The concentration of oxide impurities formed on oxidation of the Al metal must also vary across the barrier layer. Analysis of the bath solution after the anodic oxidation of Al, using an atomic absorption spectrophotometer, showed that Fe dissolves in the bath to an extent comparable to the amount of Fe impurities present in Al metal which has been converted to Al_2O_3, especially at higher T_b's and lower i's. Hence in the Al_2O_3 film only traces of Fe compounds such as Fe_2O_3 can exist. Only SiO_2 impurities are present in the oxide in small amounts, not affecting the catalytic efficiency of Al_2O_3 in the test reaction.

The stoichiometry defects, the small amount of H_2O and OH groups, and the impurities inside the barrier layer also produce a heterogeneity in the oxide nature across the barrier layer and along the pore wall surface. Nevertheless, their significance seems to be unimportant in relation to the influence exerted by the variation of both the crystallite sizes and the concentration of the incorporated SO_4^{2-}. On prolonged heating during catalysis experiments at the relatively high temperatures employed any probable influence of the incorporated H_2O/OH and the stoichiometry defects become reduced or eliminated.

3. Modification of the Nature and Structure of Porous Anodic Al_2O_3 Film Catalysts by Hydrothermal Treatment

Hydrothermal treatment of these oxides results in the hydration of oxide and in the closure of pores as described in detail previously (24). On hydration, OH groups and H_2O molecules are adsorbed on the surface of microcrystallites (24) with concomitant removal of the electrolyte anions, SO_4^{2-}, enclosed in the intercrystallite surfaces/spaces (29). Microcrystallites become separated and swell on addition of H_2O either as OH or as H_2O on their surface. A hydrated skin layer develops on the pore wall surface, the thickness of which increases with treatment time, yielding a swollen layer, as shown in Fig. 3b, which effects pore closure on prolonged hydrothermal treatment.

Complete pore closure generally occurs for films having thickness $h < h_c$ up to a specific thickness for each pair of T_b and i; H_2O retained by the oxide in this case is directly related to the pore void volume according to a ratio which is close to 1 g/cm^3 (24). There exists a position on the pore walls of a film with thickness h_c at which the complete hydration of dry material and the swelling along the direction perpendicular to the pore wall surface gives a hydrated material volume sufficient to completely fill up the initial pore void volume. This position anticipates such a film thickness h_f. The actual thickness h_f' is considerably higher than h_f and at the T_b's and i's used in the present study it approaches h_c (24). A transport of hydrated oxide, which is a moderately coherent material, may take place en masse along the pore axis, filling pores up to a length h_f'.

The swelling of hydrated material results in a change of the initial relative positions of microcrystallites, the destruction of the initial crystallite size distribution, and the "mixing" of crystallites of various sizes. These and other simultaneous structural modifications such as the removal of SO_4^{2-} from intercrystallite surfaces must be of much greater significance in the direction of the perpendicular to the pore surface than along the pore wall surface. Due to the profile of the variation of these factors across the barrier layer, the above structural modifications become of much greater importance towards the pore base.

The H_2O retained by the hydrothermally treated oxides is relatively loosely bound and easily removed on heating. Heating at, e.g., 350°C for 2 hr removes the total amount

of molecular H_2O and approximately the total amount of OH retained (24), but this is expected to take place even at significantly lower temperatures and times of heating. The same is expected to occur during heating in catalysis experiments following hydrothermal treatment. The quick removal of H_2O and OH from intercrystallite spaces and crystallite surfaces during heating is accompanied by a shrinking of the swollen hydrated material, causing the movement/rearrangement of crystallites towards their initial positions and the reformation of pores with walls consisting again of dry crystallites. However, the changes in crystallite positions, the "mixing" of crystallites of various sizes, and the removal of SO_4^{2-} during the hydration process ensure that a new pore wall material with modified structural and reactive properties is created.

The changes in the pore wall material structure which are expected to take place are as follows: (i) Crystallites remain separated to some extent. (ii) The pore shape somewhat changes and the new pore wall surface closes in towards the pore axis (pore narrowing) but despite this (iii) a higher real active surface appears. (iv) The average crystallite size of the active dehydrated layer at each point on the pore surface generally alters as compared to that of the untreated oxide, while this difference becomes progressively reduced on passing from the pore base towards pore mouths. (v) The crystallite surfaces and intercrystallite spaces become free from the presence of SO_4^{2-} and other impurities/species. (vi) A homogenization of the active surface tends to be established along pore walls.

The conditions of preparation of anodic Al_2O_3 films such as T_b are expected to affect the extent of the modification of their structural and reactive properties effected by hydrothermal treatment. For example, the increase in T_b and the concomitant enlargement of pores favours longer migrations of crystallites from their initial positions after hydration and calcining, more effective removal of incorporated SO_4^{2-}, and reduction in the preexisting pore wall surface heterogeneity.

The active real surface of modified oxides is expected to be approximately proportional to that of untreated ones. This is inferred from the comparable crystallite sizes achieved on heating during the preceding catalysis experiments inside both the whole oxide bulk and the modified layer on pore walls, even for oxides prepared at different conditions. Also, it is inferred from the fact that the thickness of the active sublayer of this layer is expected to be smaller than the total layer thickness. The true active surface, S', is lower than that of separated crystallites inside the whole modified layer. This active sublayer is located on the new pore wall surface and situated near the pore wall surface of untreated oxide. Therefore, it was decided to take the real surface S into consideration for calculations.

4. Preliminary Measurements of Catalysis over Anodic Aluminas

Formic acid decomposes in two ways: a dehydrogenation reaction, $HCOOH \rightarrow H_2 + CO_2$, or a dehydration reaction, $HCOOH \rightarrow H_2O + CO$. A blank run and a run in which Al metal was used as catalyst showed no measurable catalytic activity. In the second run traces of CO_2 were observed above 355°C. The decomposition of HCOOH on the porous anodic Al_2O_3 film catalysts used was found to be $\simeq 100\%$ dehydration. Traces of CO_2 were observed at temperatures above 355°C, which were probably due to the dehydrogenative decomposition of HCOOH taking place on the small amounts of bare Al metal surface remaining uncovered by the oxide; metals are generally dehydrogenative catalysts in the HCOOH decomposition (30). These CO_2 traces were insufficient to influence the measurements of reaction rate, which referred only to the dehydration reaction taking place on the anodic alumina.

The reaction rate was measured in $HCOOH + H_2O$ mixtures at different concentrations and temperatures over an anodic alumina catalyst prepared at 30°C, 35 mA/cm^2, and 50 min. It was found that the reaction rate was constant for HCOOH molar fraction (or HCOOH partial pressure) values higher than a specific value for each temperature, which decreased as the temperature decreased; e.g., 0.55 and 0.38 at 350 and 320°C, respectively. Below these values, reaction rate decreased with decreasing HCOOH mole fraction. The rate of HCOOH feed to the reactor chamber was regulated to be much higher than the conversion inside the reactor so that the mole fraction of HCOOH over every point of the catalyst surface was always much larger than the abovementioned values. Reaction rates, reaction time intervals, and the amount of HCOOH added into the reactor ensured that the mole fraction of HCOOH was always close to 1.

Hence, under the experimental conditions chosen, the apparent order of reaction was zero and the reaction rate (r) yielded the reaction rate constant (k) directly. The zero order of reaction suggests that the H_2O is strongly adsorbed and that the rate determining step is the H_2O desorption or, alternatively, that HCOOH is strongly adsorbed and that the rate determining step is a chemical reaction. The first supposition is not valid since a zero order reaction should be observed towards high H_2O mole fraction (low HCOOH mole fraction), which is not the case. In addition, it is known that in the range of reaction temperatures employed no molecular H_2O is adsorbed on the anodic alumina (24). The results are consistent with the latter suggestion. Hence, H_2O desorbs quickly for mole fractions higher than the above. Also, CO cannot inhibit the reaction and its desorption cannot be the rate determining step of the overall process. By IR spectros-

copy it was shown that even at significantly lower temperatures, $\leq$190°C, during HCOOH decomposition on γ-Al_2O_3 no CO, CO_2, or molecular HCOOH was present during the course of the reaction (31).

5. *Decomposition of HCOOH on Anodic Al_2O_3 Film Catalysts*

The porous anodic Al_2O_3 film catalysts which were tested in the HCOOH catalytic decomposition reaction were prepared at T_b = 25, 30, and 40°C, i = 35 mA/cm^2, and at anodization times (t), yielding film thicknesses varying from 21.6, 10.8, and 5.4 μm up to the maximum possible thicknesses, 55.5, 38, and 15.3 μm, achieved at these T_b's, respectively. The initial deactivation of catalysts, until reliable measurements could be obtained, was large, extending in some cases even up to 75% of the initial catalyst activity. It generally increased with decreasing film thickness, the lowest appearing at $t \geq t_c$.

The measurements of reaction rates at various temperatures which were performed refer to the oxide spread

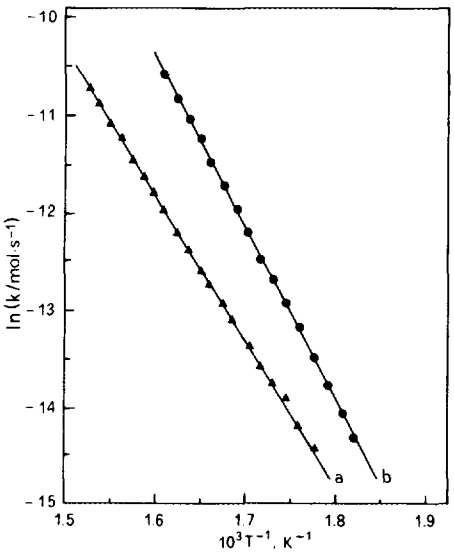

FIG. 5. Arrhenius plots for the HCOOH catalytic dehydration (a) on a porous anodic Al_2O_3 film prepared at T_b = 25°C and t = 160 min, and (b) on the same oxide film modified by hydrothermal treatment.

TABLE 1

Values of Kinetic Parameters E, k_0, and k_0/S Derived from the Catalytic Dehydration of HCOOH on Anodic Porous Al_2O_3 Films (a) and on Modified Porous Anodic Al_2O_3 Films (b) of Various Thicknesses (h), Prepared at Bath Temperatures (T_b) of 25, 30, and 40°C, Current Density 35 mA/cm^2, and Various Anodization Times (t)

No. of catalyst	T_b (°C)	t (min)	h (μm)	E (kcal · mol^{-1})		log(k_0) (mol · s^{-1})		log($k_0 \cdot S^{-1}$) (mol · s^{-1} · m^{-2})	
				(a)	(b)	(a)	(b)	(a)	(b)
1	25	20	21.6	21.3	27.3	1.07	4.38	0.78	4.09
2	25	40	43.3	27.1	33.2	3.78	6.91	3.13	6.26
3	25	60	53.8	29.4	34.5	5.07	7.54	4.31	6.78
4	25	80	55.5	29.9	36.0	5.34	8.09	4.55	7.30
5	25	120	55.5	30.3	34.3	5.48	7.48	4.70	6.69
6	25	160	55.5	29.6	34.8	5.24	7.67	4.46	6.88
Mean values for catalysts 4, 5, and 6				29.9	35.0	5.35	7.75	4.57	6.96
7	30	10	10.8	23.5	29.9	1.67	5.09	1.66	5.08
8	30	20	21.6	26.6	31.1	3.41	5.97	3.07	5.63
9	30	35	35.8	29.7	32.3	5.09	6.56	4.47	5.94
10	30	50	38.0	30.7	32.5	5.51	6.66	4.85	6.01
11	30	75	38.0	30.4	31.8	5.39	6.40	4.73	5.74
12	30	100	38.0	30.4	32.3	5.39	6.60	4.73	5.94
Mean values for catalysts 10, 11, and 12				30.5	32.2	5.43	6.55	4.77	5.90
13	40	5	5.4	24.4	30.8	1.88	5.31	2.13	5.56
14	40	10	10.8	26.7	31.4	3.31	5.86	3.22	5.77
15	40	15	14.4	30.4	31.8	5.01	6.09	4.76	5.85
16	40	20	15.3	31.6	32.3	5.43	63.1	5.16	6.03
17	40	40	15.3	31.4	31.7	5.37	6.10	5.10	5.83
18	40	60	15.3	32.3	31.5	5.69	6.02	5.42	5.74
Mean values for catalysts 16, 17, and 18				31.8	31.9	5.50	6.14	5.23	5.87

over the 33 cm^2 geometric surface area of the oxidized Al metal. From the measurements of the rate of the zero order reaction at various temperatures for each catalyst, the activation energy (E) and frequency factor (k_0) were determined.

Figure 5a depicts a typical Arrhenius plot obtained from an oxide catalyst prepared at T_b = 25°C and t = 160 min. For all catalysts used, satisfactory straight lines were always obtained with a correlation coefficient >0.993. The kinetic parameters E, log k_0 and log (k_0/S) obtained are cited in Table 1. All of them increase with anodization time up to a time which is beyond t_1 and up to t_c. Beyond t_c, they remain approximately constant. The variation of both E and k_0/S confirms the heterogeneity of the pore wall surface. When Al_2O_3 film catalysts with the same thickness are compared, it appears that all the above parameters increase with increasing T_b. This change in E and log(k_0/S) confirms that the pore surface heterogeneity arises also with a variation in T_b. The average maximum limiting values of the above parameters do not significantly differ for the various T_b's. All of them show only a small tendency to increase with increasing T_b.

Three specific activities can be defined, r/S_g, r/m, and r/S. The variation of these activities at reaction temperature

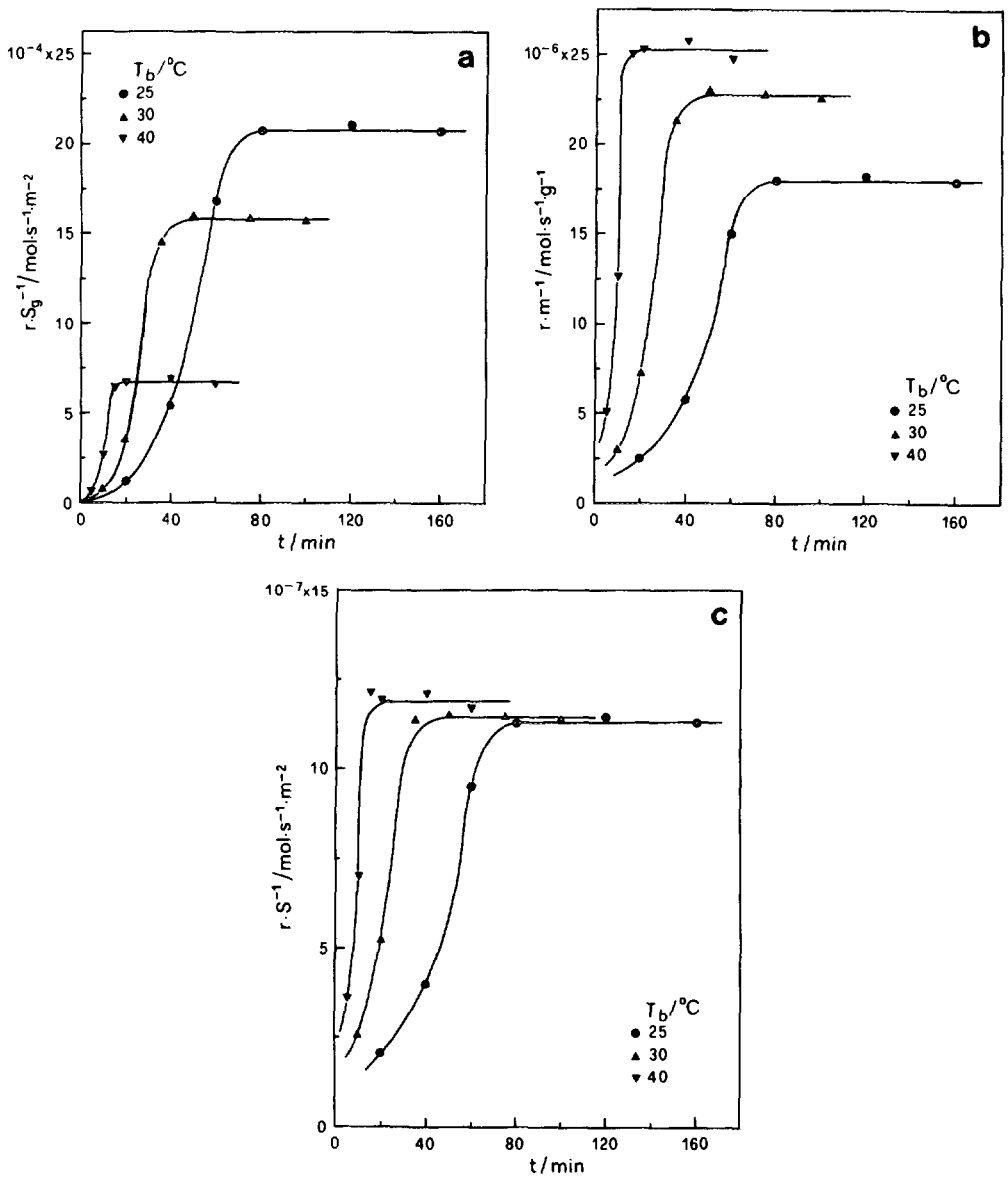

FIG. 6. Dependence of the activities (a) r/S_g, (b) r/m, and (c) r/S of porous anodic Al_2O_3 films in the HCOOH catalytic dehydration at 350°C on anodization time t at T_b 25, 30, and 40°C.

350°C with t at various T_b's is shown in Fig. 6. For the activity r/S_g an inflection point appears at time $\simeq t_1$. Beyond t_c, r/S_g remains approximately constant. For the same thickness of films, the activity increases with T_b, due mainly to the fact that the total real surface of the oxide corresponding to the S_g geometric surface film area also changes in a similar way. The maximum limiting activity increases with decreasing T_b, primarily due to a similar increase in both h_c and S.

A qualitatively similar dependence of r/m and r/S activities on t is observed. Generally, T_b exerts a positive effect on these activities. For r/m this is true either when Al_2O_3 film catalysts of the same thickness or films with the maximum limiting thickness are compared. The above are also valid for the activity r/S but its maximum limiting value shows only a slight tendency to increase with T_b. For $t < t_c$, on the other hand, a considerable rise in r/S with t and T_b is again observed.

The variation of r/S at reaction temperature 350°C vs h is shown in Fig. 7. An accelerated increase in r/S with thickness is verified. At each film thickness considered, r/S increases significantly with T_b. The r vs. S variation is shown in Fig. 8. Both the r and the dr/dS parameters increase strongly with S and T_b. Also, they both increase with film thickness as well as with T_b for each given h value. If we consider a ring-shaped differential surface, dS, on the pore wall surface, Fig. 3a, with a ring diameter (HI) at a distance h from the pore base, then its activity should be given by the factor $(nS_g)^{-1}(dr/dS)$ and vary similarly with dr/ds.

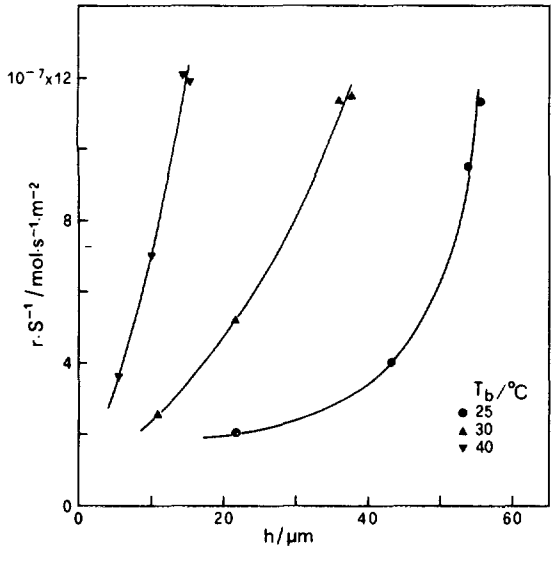

FIG. 7. Variation of the activity r/S of porous anodic Al_2O_3 films in the HCOOH catalytic dehydration at 350°C with film thickness at T_b 25, 30, and 40°C.

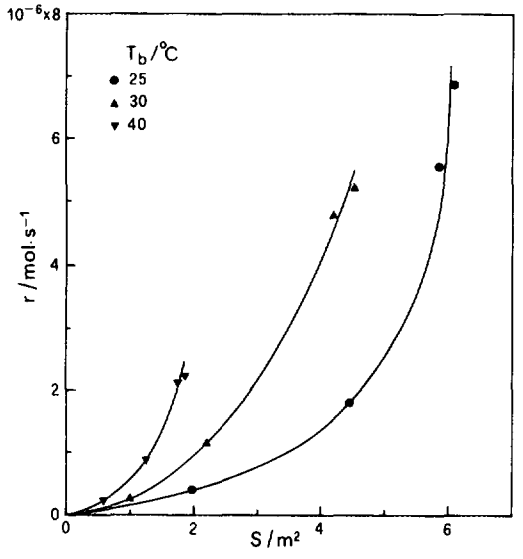

FIG. 8. Reaction rate dependence of HCOOH dehydration at 350°C exhibited by porous anodic Al_2O_3 films with a constant geometric surface area of 33 cm^2 on the total pore wall surface area at T_b 25, 30 and 40°C.

6. *Decomposition of HCOOH on Modified Anodic Al_2O_3 Film Catalysts*

An initial deactivation of catalysts was also observed as in the case of untreated oxide catalysts. It also increased generally with decreasing film thickness, but it was much lower, being always ≤35–40%. A typical Arrhenius plot of the HCOOH catalytic decomposition reaction on hydrothermally modified anodic Al_2O_3 films is shown in Fig. 5b for a film prepared at T_b = 25°C and t = 160 min. The kinetic parameters E, log k_0, and log(k_0/S) of HCOOH decomposition on the modified catalysts are given in Table 1.

All the above parameters increase with t up to t_c and then remain constant as in the case of untreated oxide catalysts, but the span of their variation is lower than that of untreated oxides, especially at the higher T_b's. At each T_b, all the above parameters become significantly higher than those of untreated oxides for the lower film thicknesses. For films having the maximum limiting thickness all parameters also become considerably higher, except for E at T_b's 30 and 40°C, where it becomes only slightly higher. When films of the same low thickness are compared all parameters generally increase on increasing T_b. The values for films with the maximum limiting thicknesses are comparable for T_b's 30 and 40°C, but they are appreciably higher at T_b = 25°C. Although the span of their variation with film thickness at T_b = 25°C is generally lower than that of the untreated oxides, it remains remarkable.

The variation of activities r/S_g, r/m, and r/S at reaction

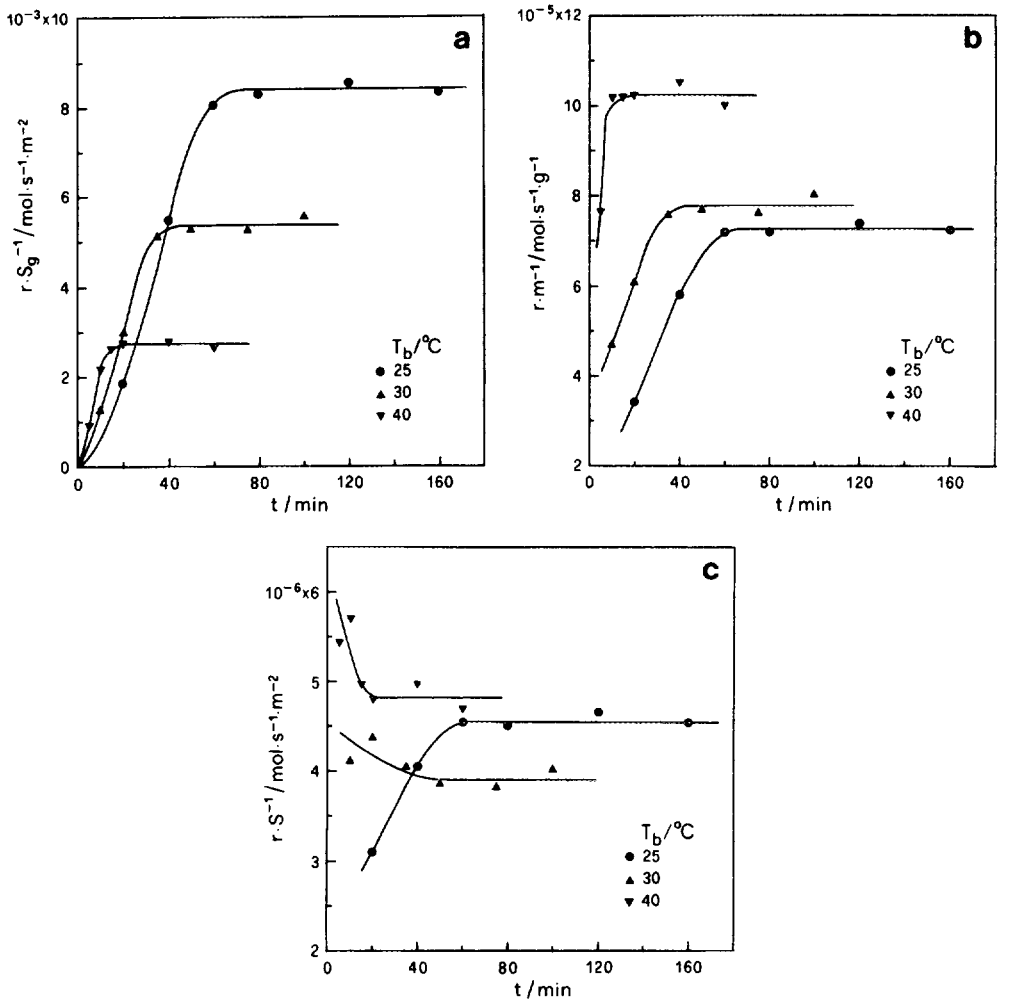

FIG. 9. Dependence of the activities (a) r/S_g, (b) r/m, and (c) r/S of porous anodic Al_2O_3 films modified by hydrothermal treatment in the HCOOH catalytic dehydration at 350°C on anodization time t at T_b 25, 30, and 40°C.

temperature 350°C with t for the T_b's used is shown in Fig. 9. Their values are much higher than those for untreated oxide catalysts. The dependence of r/S_g and r/m on t and T_b is qualitatively similar to that of untreated oxides; however, the variation of r/S with t and T_b is much different. For T_b = 30°C its value is approximately identical for all t's showing an almost complete homogenization of active surface. A perceptible increase in the r/S value with decreasing t for $t \leq t_c$ at T_b = 40°C is observed. At T_b = 25°C the appreciable increase in the r/S value with t up to t_c shows again that some heterogeneity along the pore walls persists.

The promotion factor (pf) determined as the ratio of the rate of HCOOH decomposition obtained by the modified oxide to that obtained by the untreated oxide at a reaction temperature of, e.g., 350°C, varies with t at the T_b's used as shown in Fig. 10. It decreases strongly with t up to t_c and then remains constant for each T_b. The ultimate value of pf at $t \geq t_c$ is essentially identical for all T_b's. It is noteworthy that *pf* rises from ≃4 up to values exceeding 10 on passing from the maximum limiting film thicknesses to the lower ones used. For the same film thickness pf increases considerably with decreasing T_b. It was found also to increase with a rise in reaction temperature.

7. *Interpretation*

An interpretation of the catalytic behaviour of anodic Al_2O_3 films is offered below. The two main factors determining pore wall surface heterogeneity act as follows. A decrease in crystallite size causes an increase in both the adsorption enthalpy of species implicated in the slow step of the HCOOH decomposition reaction (hence, an increase in the activation energy is expected) and the fre-

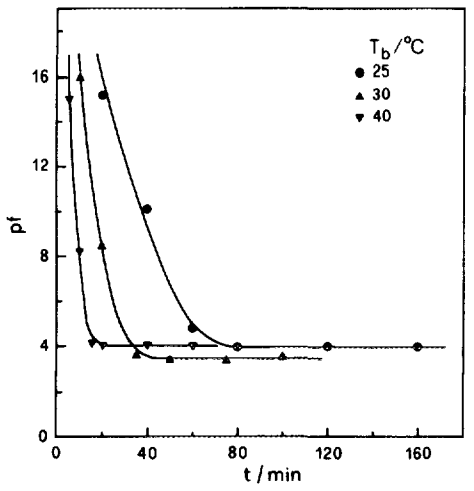

FIG. 10. Variation of promotion factor at reaction temperature 350°C with anodization time t at T_b 25, 30, and 40°C.

quency factor, finally making a net positive contribution to surface activity. The SO_4^{2-} anions present in intercrystalline surfaces appear to inhibit the reaction, probably by occupying active Lewis acidic sites, which seem to be the active centres for HCOOH decomposition, causing the diminution of parameters E, k_0/S, and r/S. At any point on the pore wall surface, the lower the crystallite size and the lower the concentration of SO_4^{2-} in intercrystalline surfaces the higher become the values of E, k_0/S, and r/S.

The initial catalyst deactivation cannot be regarded as a poisoning of catalysts or an advancing inhibition of the reaction by the products, since they desorb quickly (24, 31). It is attributed to the simultaneous procesess of (i) the coagulation of the very active crystallites of low sizes, which become prone to coagulation during heating in catalysis experiments, and (ii) the increase in the SO_4^{2-} concentration in the intercrystalline surfaces and even on the pore wall surface, which obviously follows the extensive reduction of intercrystalline surface area. These processes take place until crystallite sizes inside the whole oxide mass acquire comparable magnitudes up to a limit depending on the heating temperature. Crystallites are probably not of the same size, as their final size must also be influenced by the local SO_4^{2-} concentration.

The increase in the SO_4^{2-} concentration in intercrystalline surfaces occurs since SO_4^{2-} is adsorbed only on them, not being removable in the temperature range employed in the catalysis experiments (32), and since its size is much larger than that of O^{2-}. Thus SO_4^{2-} ions cannot occupy O^{2-} sites in the crystal lattice of microcrystallites and their larger size also prohibits their diffusion from SO_4^{2-}-enriched to SO_4^{2-}-poor regions inside the oxide bulk. The crystallite digestion is probably assisted also by the removal of the small amount of OH and H_2O initially present in intercrystallite surfaces on heating.

The lower crystallite size is accompanied by an increasing rate of crystallite size growth and a greater relative final extent of crystallite digestion. The SO_4^{2-} concentration in intercrystallite surfaces becomes, accordingly, enhanced and finally much larger than the initial SO_4^{2-} concentration. Hence, the deactivation rate and its final extent gradually diminish towards pore mouths and on average over the whole pore wall surface with increasing film thickness, which was indeed shown by the experimental results.

After initial catalyst deactivation, crystallites acquire comparable sizes along the pore wall surface even for films prepared at various T_b's. The SO_4^{2-} concentration in intercrystallite surfaces appears to be much higher than its initial value at the pore base surface and it gradually decays towards pore mouths up to around point P in Fig. 3a. Also, at the pore base surface, the more pronounced relative enlargement of crystallite size also causes the SO_4^{2-} concentration in intercrystallite surfaces to increase with decreasing T_b. Thus it increases on average along the pore wall surface for films having identical or the maximum limiting thicknesses.

Hence, the local values of the parameters E, k_0/S, and r/S at each point on the pore wall surface must increase from the pore base towards the pore mouths or on average with film thickness. Also, a decrease in T_b must cause a decrease in these kinetic parameters for films having either identical or the maximum limiting thicknesses. For films with the maximum limiting thicknesses at various T_b's the conical shape of pores and probably the increasing percentage, PB/AB, of the surface free of electrolyte anions, which becomes significant due to the conical shape of pores as T_b decreases, extensively reduce the existing differences in kinetic parameter values. These become comparable and have only a slight tendency to increase with T_b. The above variation of kinetic parameters with film thickness and T_b is indeed that shown by the results of the HCOOH decomposition.

The deactivation of hydrothermally treated oxide catalysts is different in nature from that of untreated ones. The separated microcrystallites approach each other during their dehydration on heating. Irrespectively of a probable coagulation tendency to form crystallites of larger average size, the real active surface of crystallites decreases somewhat with operation/heating time as their progressive approach results in both the increase of the contact surface area between crystallites and the creation of isolated intercrystallite voids not accessible to HCOOH molecules until a steady state is achieved. This rearrangement of crystallites and diminution in real surface proba-

bly takes a longer time than the complete dehydration of crystallite surfaces.

In the modified oxides microcrystallites become separated and liberated from the presence of SO_4^{2-} to a significant extent so that the crystallite size arises as the main factor determining the catalytic behaviour of oxide for each film thickness; separated crystallites appear to be "quasi-isolated," giving higher E, k_0/S, and r/S values in comparison to those of the untreated oxides. The increase in their values becomes greater for lower film thicknesses. For identical film thicknesses the sequence of the variation of E, k_0/S, and r/S with T_b remains generally similar to that for the untreated oxides; i.e., they diminish with decreasing T_b. The concomitant narrowing of pores prevents extensive migration of crystallites and their complete disengagement from the presence of SO_4^{2-}.

Despite the average crystallite size becoming probably slightly smaller with lowering T_b, the expected increase in E, k_0/S, and r/S is surpassed by the opposite action of the still remaining SO_4^{2-}, resulting finally in the observed sequence. For films with the maximum limiting thickness the trend seems to become reversed in comparison to the untreated oxides. Thus higher E and k_0/S are obtained at lower T_b's although at T_b's 30 and 40°C they attain comparable values. This may be due to the somewhat lower crystallite sizes on average on pore walls in connection with the increased portion of pore wall surface initially free of SO_4^{2-}, PB/AB in Fig. 3a, so that their influence predominates over the opposite influence of the SO_4^{2-} that remains inside the dehydrated layer on pore walls, being effective for film thicknesses up to $\approx NP$.

For the same films, the variation of the values of r/S, which are comparable for the various T_b's, is dissimilar to the variation of E with T_b; however, taking into consideration the true active surface S', it is expected that r/S' as well as k_0/S' vary similarly to E with t and T_b. Generally, the different profile of the r/S vs t and T_b variation from that of E vs t and T_b in the modified catalysts and the different manner of variation of r/s vs t at various T_b's are due to the different extent of structural modifications of pore wall material. They are also due to the fact that the ratio S'/S is variable along the pore wall surface and also with T_b, arising from a concurrent variation of crystallite sizes and of the thickness of both the modified and effective layers.

8. *The Mechanism of HCOOH Catalytic Decomposition*

The catalytic decomposition of HCOOH on chemically prepared γ-Al_2O_3 was also investigated earlier (22, 31, 33) by means of IR spectroscopy at reaction temperatures $\leq$190°C and a nearly complete dehydration reaction was verified. When γ-Al_2O_3 is exposed to HCOOH vapour, formate ions and protons are formed by the dissociative adsorption of HCOOH. During the decomposition of HCOOH on γ-Al_2O_3 the chemisorbed species were formate ions, protons, and H_2O, while no CO nor HCOOH molecules were adsorbed under the experimental conditions (22, 31). The decomposition of HCOOH was regarded as taking place in two stages (33).

In the initial stage, the reaction rate was found to be linearly dependent both on the HCOOH ambient partial pressure and on the fraction of surface Lewis acidic sites not occupied by adsorbed H_2O; the reaction rate is depressed sharply by the adsorption of H_2O and the mechanism involves gaseous HCOOH molecules colliding with formate ions adsorbed on Lewis acidic sites and producing CO, while the Lewis acidic sites are destroyed by the product H_2O. Then, during the stationary state, the reaction rate was found to be linearly dependent on both the HCOOH ambient partial pressure and the surface concentration of Brønsted acidic sites (protons supplied by the dissociative adsorption of HCOOH); the reaction is inhibited by the product H_2O and the mechanism involves interaction between HCOOH molecules and Brønsted acidic sites.

The surface formate ion was stable and decomposed in vacuum mainly to H_2O and CO, but only at temperatures considerably higher than those at which HCOOH decomposition took place. The decomposition rate of the formate species on the alumina catalyst in vacuum was about two orders of magnitude lower than the rate of decomposition of HCOOH vapour at the same temperature and surface coverage (22, 31). These results proved that the decomposition of HCOOH via the decomposition of a formate ion has a higher activation energy than the decomposition via the interaction of HCOOH with the surface protons and anticipated that the reaction may proceed through the formate ion decomposition at much higher temperatures, where it can become the predominant mechanism of reaction.

The latter are in good agreement with the results of the present study, which postulate that the reaction takes place mainly via a formate ion decomposition mechanism, for the following reasons. (i) In the present study no measurable rate of reaction was observed at temperatures $\leq$190°C by the method employed. (ii) The HCOOH decomposition in the present work took place at considerably higher temperatures, 270°C $< T <$ 390°C. (iii) Measurable rates of reaction were always observed above 270°C. (iv) The activation energy is indeed generally high, varying from 21 up to 36 kcal/mol. (v) At these temperatures no molecular H_2O can exist on the anodic alumina surfaces (24) and so H_2O cannot be implicated in the aforementioned mechanisms via the interaction of HCOOH in the gaseous phase with formate ions and Brønsted acidic sites on the alumina surface. (vi) At these

temperatures not only is molecular H_2O absent from the surface of the anodic alumina but also approximately the total amount of the preexisting protons is removed (24). If a small number of protons are considered as remaining on the pore wall oxide surface or on the microcrystallite surfaces in the reaction temperature range 270–390°C, they must be strongly adsorbed and hence be unable to act as active Brønsted acidic sites capable of causing the HCOOH decomposition. During the reaction, OH groups on the alumina surface are formed by the dissociative adsorption of HCOOH and the decomposition of formate ions. They are quickly condensed into H_2O and desorbed.

Thus, the reaction must predominantly take place via a mechanism involving a formate ion intermediate, according to the following steps. (i) Dissociative adsorption of HCOOH saturating the surface (fast step) as the zero order of the reaction, as the experimental conditions used indicate and as molecular HCOOH is not present on the alumina surface even at much lower temperatures. (ii) Formate ion decomposition (slow step) giving CO product, which is easily desorbed, since it was not detected on the alumina surface even at much lower temperatures (31, 33). This slow step is in agreement with earlier findings (22, 31). After the decomposition of formate ions hydroxyl groups remain on the surface. Neighbouring OH groups are easily condensed into H_2O (fast step), which is easily removed, as at these temperatures molecular H_2O cannot exist on the anodic alumina surfaces (24).

It is apparent that the slow step of the decomposition of each HCOOH molecule takes places on a Lewis acidic site, Al^{3+}. The mechanism of HCOOH decomposition can be described schematically by the following steps:

1. HCOOH adsorption (fast step):

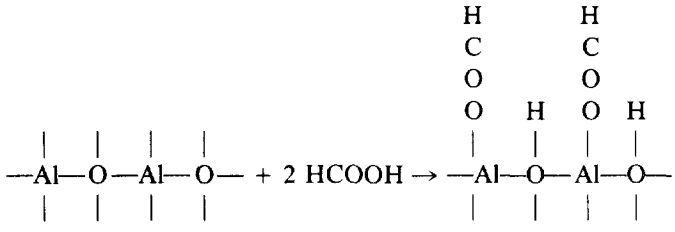

2. Formate ion decomposition (slow step) yielding CO which quickly desorbs:

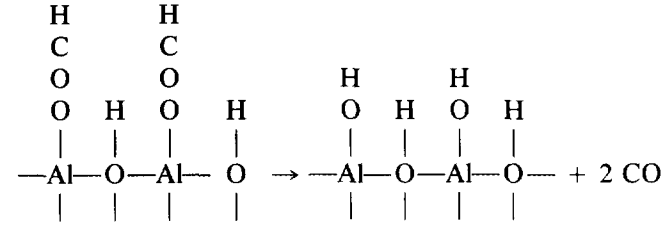

3. Hydroxyl ions condensation (fast step) yielding H_2O which quickly desorbs:

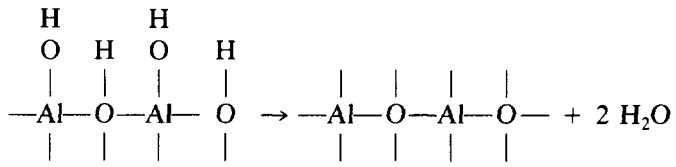

This mechanism implies that the promotion of catalytic activity of anodic Al_2O_3 achieved by hydrothermal treatment cannot be attributed to the small quantity of preexisting OH groups remaining on crystallite surfaces since they do not participate in the mechanism and they do not exert any direct influence on the catalytic efficiency of the active crystallite surfaces. The promotion is ascribed to the separation of crystallites, to the removal of SO_4^{2-}, and to the increase of surface concentration and intensity of active centres. An indirect positive influence of the preexisting OH groups could be attributed to the fact that their presence assists crystallites to remain separated.

CONCLUSIONS

From the results of the present study the following conclusions can be drawn:

1. The structure of porous anodic Al_2O_3 films can be well described and designed as regards features such as pore surface density, pore base and pore mouth diameter, length of pores, shape of pores, porosity, and total and specific real surface area. The choice of appropriate conditions for the electrochemical preparation of anodic aluminas can produce the desired structure.
2. The anodic aluminas are dehydration catalysts for formic acid decomposition.
3. The nature of the oxide across the pore wall material and along the pore wall surface is heterogeneous, with a regular and well described pattern. This heterogeneity results in a significant change in catalytic effectivity and in the relevant kinetic parameters along the pore wall surface. The conditions of the anodic alumina preparation significantly affect the above heterogeneity and variability of catalytic efficiency and kinetic parameters.
4. The anodic alumina was proved to be an effective catalyst, primarily due to the electrochemical method of preparation and to its microcrystalline nature.
5. Hydrothermal treatment of porous anodic aluminas extensively modifies their nature and structure. The microcrystallites composing the pore wall material become separated and incorporated species such as SO_4^{2-} in intercrystallite surfaces are removed, with the result that a homogenization of the pore wall surface along pores tends to be established.

6. Modified anodic aluminas prevented the initial deactivation to a significant extent and showed much higher catalytic efficiencies than those of the untreated anodic aluminas. The promotion factor at the intermediate reaction temperature of 350°C was found to increase from ≈4 up to values exceeding 10. At higher reaction temperatures the promotion factor becomes even higher.

7. Anodic aluminas appear to possess very interesting catalytic properties stimulating further investigation. Their well designed structure serves to show that they can be used as model catalysts or supports.

REFERENCES

1. Young, L., "Anodic Oxide Films." Academic Press, London, 1961.
2. Diggle, J., Downie, T., and Goulding, C., *Chem. Rev.* **69,** 365 (1969).
3. Cocke, D. L., Johnson, E. D., and Merrill, R. P., *Catal. Rev. Sci. Eng.* **26,** 163 (1984).
4. Ruckenstein, E., and Malhotra, M., *J. Catal.* **41,** 303 (1976).
5. Chu, Y., and Ruckenstein, E., *J. Catal.* **55,** 281 (1978).
6. Ruckenstein, E., and Chu, Y., *J. Catal.* **59,** 109 (1979).
7. Chen, J., and Ruckenstein, E., *J. Catal.* **69,** 254 (1981).
8. Rai, K., and Ruckenstein, E., *J. Catal.* **40,** 117 (1975).
9. Chu, Y., and Ruckenstein, E., *J. Catal.* **41,** 384 (1976).
10. Honicke, D., *Appl. Catal.* **5,** 197 (1983).
11. Honicke, D., *Appl. Catal.* **5,** 199 (1983).
12. Glassl, H., Kramer, R., and Hayek, K., *J. Catal.* **63,** 167 (1980).
13. Glassl, H., Kramer, R., and Hayek, K., *J. Catal.* **68,** 388 (1981).
14. Glassl, H., Hayek, K., and Kramer, R., *J. Catal.* **68,** 397 (1981).
15. Glassl, H., and Hayek, K., *Thin Solid Films* **89,** 413 (1982).
16. Skoulikidis, Th., and Sarropoulos, C., *in* "Proceedings of 4th International Congress for the Study of Bauxites, Alumina and Aluminium," Vol. 3, p. 356, National Technical University, Athens, 1978.
17. Skoulikidis, Th., and Patermarakis, G., *Aluminium* **65,** 185 (1989).
18. Thomson, G. E., Furneaux, R. C., and Wood, G. C., *Corros. Sci.* **18,** 481 (1978).
19. Trillo, J., Munuera, G., and Criado, J., *Catal. Rev.* **7,** 51 (1973).
20. Patermarakis, G., Lenas, P., Karavassilis, Ch., and Papayiannis, G., *Electrochim. Acta* **36,** 709 (1991).
21. Ai, M., *J. Catal.* **50,** 291 (1977).
22. Noto, Y., Fukuda, K., Onishi, T., and Tamaru, K., *Trans. Faraday Soc.* **63,** 2300 (1967).
23. Anderson, R. B., and Dawson, P. T., *in* "Experimental Methods in Catalytic Research" (R. B. Anderson, Ed.), Vol. 1, p. 10. Academic Press, London, 1968.
24. Patermarakis, G., and Kerassovitou, P., *Electrochim. Acta* **3,** 125 (1992).
25. Patermarakis, G., and Papandreadis N., *Electrochim. Acta* **38,** 1413 (1993).
26. Baker, B., and Pearson, R., *J. Electrochem. Soc.* **119,** 160 (1972).
27. Parkhutik, V. P., *Corros. Sci.* **26,** 295 (1986).
28. Bernard, W. J., and Russell, P. G., *J. Electrochem. Soc.* **127,** 1256 (1980).
29. Murphy, J., *in* "Proceedings, Anodizing Aluminium Symposium," p. 3. Birmingham, UK, Aluminium Development Association, London, 1967.
30. Bond, G., "Catalysis by Metals." Academic Press, London, 1962.
31. Tamaru, K., "Dynamic Heterogeneous Catalysis." Academic Press, London, 1978.
32. Sharma, A. K., and Bhojaraj, H., *Plat. Surf. Finish.* **76,** 59 (1989).
33. Fukuda, K., Noto, Y., Onishi, T., and Tamaru, K., *Trans. Faraday Soc.* **63,** 3072 (1967).